

Journal of Geophysical Research: Earth Surface

RESEARCH ARTICLE

10.1002/2013JF002894

Key Points:

- Hydrogeology of proglacial lakes can be driven by glacial recharged groundwater
- Talik evolution is dependent on advective heat transport by groundwater flow
- Regional-scale hydrogeology in permafrost is influenced by open taliks

Correspondence to:J. M. Scheidegger,
j.scheidegger@uea.ac.uk**Citation:**Scheidegger, J. M., and V. F. Bense (2014), Impacts of glacially recharged groundwater flow systems on talik evolution, *J. Geophys. Res. Earth Surf.*, 119, 758–778, doi:10.1002/2013JF002894.

Received 19 JUN 2013

Accepted 7 FEB 2014

Accepted article online 12 FEB 2014

Published online 2 APR 2014

Impacts of glacially recharged groundwater flow systems on talik evolution

J. M. Scheidegger¹ and V. F. Bense¹¹School of Environmental Sciences, University of East Anglia, Norwich, England

Abstract Most currently permafrost-covered landscapes underwent fundamental shifts in the hydrogeological and the thermal regime as a result of deglaciation after the Last Glacial Maximum (LGM). The transient effects of heat and fluid flow associated with retreating ice sheets are important to consider for the present-day hydrogeology of these regions. In this paper, we use numerical models to evaluate the evolution of taliks underneath proglacial lakes during deglaciation. In our models, the hydrological and thermal boundary conditions at the lake site are constraint by the hydrogeological impacts of ice sheet dynamics since the LGM. During the LGM, the ground surface was insulated from air temperatures, and as a result, there was no permafrost underneath the wet-based ice. Subsequently, ice sheet retreat led to an exposure of a proglacial area to subzero air temperatures and the formation of permafrost. Where proglacial lakes form, discharge of deeper groundwater becomes focused. In this scenario, subpermafrost groundwater flow is driven by a combination of direct subglacial recharge and elevated hydraulic heads preserved in that part of the aquifer. Advective heat flow can delay or prevent through taliks from freezing as function of aquifer properties. The presence and evolution of through taliks in thick permafrost can create complex and transient hydrogeological phenomena.

1. Introduction

Taliks, unfrozen zones within the confining permafrost, are important features to consider in permafrost hydrogeology, because they connect subpermafrost aquifers to the surface hydrology system. Classically, taliks are believed to occur underneath sufficiently large surface water bodies, where thermal surface isolation is sufficient for a through talik to develop [e.g., *Sloan and Van Everdingen*, 1988; *Burn*, 2002], here referred to as a “conductive talik” (Figure 1a). The combination of heat transport through heat conduction and heat advection can result in the occurrence of “conductive-advection taliks,” where heat advection thermally erodes permafrost and can prevent or delay taliks from freezing (Figure 1b).

In permafrost-covered regions, recharge and discharge can only occur through unfrozen zones, which can either be found under insulating surface water bodies or under wet-based ice [e.g., *Andersen et al.*, 2002; *Haldorsen et al.*, 2010]. *Bense et al.* [2012] suggest that recharge in a thawing permafrost environment is not sufficient for advective heat flow to have a significant impact on permafrost degradation in a nested groundwater flow system. In contrast, advective heat flow can influence transient taliks, where geothermal heat flow anomalies occur, where flow is strongly focused, or where the recharge is not limited by effective rainfall, such as glacial recharge [*Bense et al.*, 2012; *Scheidegger et al.*, 2012].

Proglacial areas in front of a wet-based glacier or an ice sheet could be influenced by groundwater, where subpermafrost groundwater flow is driven by high hydraulic head gradients at the base of the ice sheet. Subglacial-recharged groundwater flow paths can extend into the proglacial area, where upwelling to the surface can potentially occur via localized high permeability zones [*Boulton et al.*, 1993; *Piotrowski*, 2006; *Grasby et al.*, 2012], as observed in springs found in Svalbard [*Haldorsen et al.*, 2010] or on Ellesmere Island in the Canadian High Arctic [*Grasby et al.*, 2012; *Scheidegger et al.*, 2012]. The presence of an ice sheet and the ice sheet history influences the hydrogeology, the thermal regime, and isostatic rebound. As a result of ice sheet-driven change in hydraulic head gradients, permafrost distribution, and isostatic rebound, the groundwater flow field is in a transient state over millennia, [*Bense and Person*, 2008; *Lemieux et al.*, 2008a, 2008b, 2008c].

The evolution of taliks underneath proglacial lakes near an ice margin might not be fully understood with either a heat conduction-only model [*Ling and Zhang*, 2003] or a local-scale model including heat and fluid

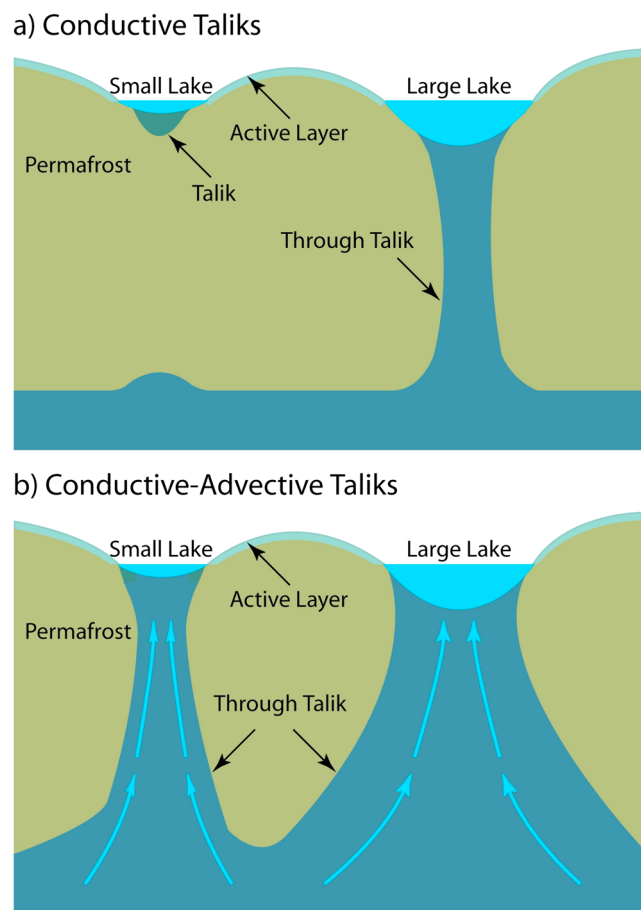


Figure 1. (a) “Conductive taliks” are formed through surface insulation alone. (b) A combination of surface insulation and heat advection of groundwater flow forms “conductive-advective taliks.”

flow [Rowland *et al.*, 2011; Grenier *et al.*, 2013]. The latter two studies use a local-scale model domain with a topography-controlled hydraulic gradient across the model domain, driving groundwater flow either into or out of a lake. Modeling results show a large impact of advective heat flow on talik evolution; for a warming scenario, advective heat flow accelerates permafrost degradation [Rowland *et al.*, 2011], and for a cooling scenario, talik closure is delayed [Grenier *et al.*, 2013].

In order to improve our understanding of talik evolution and groundwater movement in proglacial areas, we carried out a modeling study that considers coupled heat and fluid flow including ice/water phase changes, where the local boundary conditions are derived from the larger-scale dynamics of a moving ice sheet. This combines the approaches used by Bense and Person [2008] and Lemieux *et al.* [2008b], with those of Rowland *et al.* [2011] and Grenier *et al.* [2013], where a regional-scale model of a retreating ice sheet provides the boundary conditions for the transient hydraulic head and temperature distribution for simulating the thermal regime and hydrogeology in a talik beneath a proglacial lake. Thus, the modeling approach of combining a large-scale model with a local talik model considerably expands on those models in which a steady hydraulic head gradient is used to drive fluid flow as presented by Rowland *et al.* [2011] and Scheidegger *et al.* [2012]. This model allows the investigation of the role of transient advective heat flow on talik evolution.

2. Numerical Modeling

Nowadays, a number of numerical modeling codes are capable of considering the impact of ice/water phase changes on groundwater flow. These include, for example, SUTRA-ICE [McKenzie *et al.*, 2007; Ge *et al.*, 2011], ARCHY [Rowland *et al.*, 2011], and FlexPDE [Bense and Person, 2008; Bense *et al.*, 2009, 2012; Scheidegger *et al.*, 2012]. In this study FlexPDE is used, which is a flexible numerical solution environment for partial differential equations using a scripting language [PDE Solutions, 2006].

2.1. Fluid Flow

In the model, we use fully saturated fluid flow described by Darcy's law. The transient hydraulic head (h [m]) field is calculated assuming

$$\nabla \cdot [k_{rw} K \nabla h] = S_s \frac{\partial h}{\partial t} \quad (1)$$

where K (m s^{-1}) is the hydraulic conductivity and S_s (m^{-1}) the aquifer-specific storage. Where all pore fluids are frozen, hydraulic conductivity will tend toward zero, because there is no fluid available to move through the matrix. Experimental data presented by *Kleinberg and Griffin* [2005] suggest that permeability reduction (k_{rw}) can be described as a function of water saturation state

$$k_{rw} = \frac{p_w^4}{(1 + (1 - p_w)^{0.5})^2} \quad (2)$$

where the water saturation state ($p_w = \theta_w/n$) is defined from the water content θ_w [-] and porosity n [-]. However, a lower limit is set for $p_w = \sim 2\%$, resulting in a permeability reduction of 8 orders of magnitude to stabilize the numerical code [*Bense et al.*, 2009].

Hydraulic conductivity decreases with depth and results in a weakened regional flow and an increase in penetration depth of local flow systems of a nested groundwater flow system [*Jiang et al.*, 2009; *Cardenas and Jiang*, 2010]. An exponential decay model, assuming locally isotropic conditions, is used to calculate a spatially variable hydraulic conductivity $K(x, z)$ (m s^{-1})

$$K(x, z) = K_0 \exp[-B(h_s(x) - z)] \quad (3)$$

where K_0 is the hydraulic conductivity at the surface, B is a decay component which indicates the decrease rate of K with depth, h_s the surface elevation, and z is the depth [*Jiang et al.*, 2009; *Cardenas and Jiang*, 2010]. Here a value of $B = 0.001 \text{ m}^{-1}$ is used, which is within the range of 0 to 0.01 m^{-1} as suggested by *Cardenas and Jiang* [2010]. Applying the value for the decay component ($B = 0.001 \text{ m}^{-1}$) in equation (3) results in a slight increase in penetration depth of local groundwater flow as compared to models not considering a decline of permeability with depth. This value seems appropriate for a basin with a depth of about 1000 m [*Cardenas and Jiang*, 2010], such as the one considered here. The effects of assuming a declining permeability with depth are discussed in more detail for generic basins in *Jiang et al.* [2009] and *Cardenas and Jiang* [2010]. An increase in penetration depth will potentially influence the amount of advective heat transport by subpermafrost groundwater.

2.2. Heat Flow

Temperature (T [$^\circ\text{C}$]) distributions are calculated using the advection-diffusion equation, including the transient effects of the latent heat of fusion (L_i [J m^{-3}]) to simulate freezing and thawing, as follows:

$$\nabla \cdot [\kappa_a \nabla T] - C_w \vec{q} \cdot \nabla T = C_a \frac{\partial T}{\partial t} + L_i \frac{\partial \theta_w}{\partial t} \quad (4)$$

where C_a ($\text{J m}^{-3} \text{ K}^{-1}$) is the effective heat capacity of the rock/water/ice mixture, κ_a ($\text{W m}^{-1} \text{ K}^{-1}$) is the effective thermal conductivity, θ_w [-] is the water content, and $\vec{q} = -K \nabla h$ is the Darcy flux (m s^{-1}) coupled with equation (1). The first term in the left-hand side of equation (4) describes diffusive heat transport and the second term heat advection by groundwater flow. For a given aquifer porosity (n [-]) the ice content (θ_i [-]) follows the porosity, water content as $\theta_i = n - \theta_w$, and the solid-grain fraction (θ_s [-]) is equal to $1 - n$. Using these fractions, C_a is calculated as a volumetric weighted mean of the heat capacities of water, ice, and bedrock. Effective thermal conductivity, κ_a , is calculated as a weighted geometric mean from the thermal conductivities of water, ice, and bedrock [*Cutler et al.*, 2000].

The temperature interval over which freezing occurs, the freezing interval, has to be defined. Recently, *Kurylyk and Watanabe* [2013] reviewed the various options for the representation of the freezing interval in mathematical models such as the one we use here. The exact shape of the relationship between water content and temperature and the temperature range over which the freezing process occurs is a function of rock type and total porosity. Experimental data show that for most rock types, and completely fresh water, freezing of the water in pore space will be complete at -3°C . The most common functions to describe this transition are either piecewise linear or follow a power or exponential function [e.g., *McKenzie et al.*, 2007].

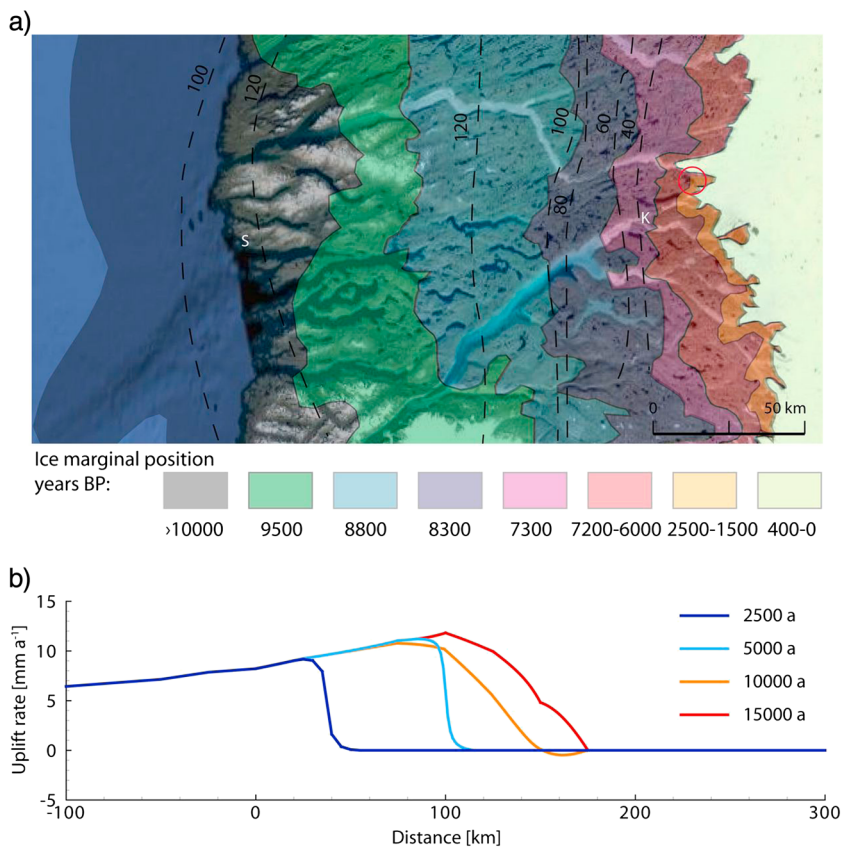


Figure 2. (a) Recession of the inland ice and postglacial uplift between Sisimut (S) and Kangerlussuaq (K) with ice position and isostatic uplift [after Scholz and Grottenthaler, 1988]. Note that between 6000 and 4000 years B.P., the ice margin was behind its present position, followed by a readvance period. (b) Uplift rates for different times implemented into model B with time is given in simulation time. The ice sheet is retreating before 11,000 years simulation time and advancing between 12,000 and 14,000 years simulation time, and stagnant thereafter. The origin on the horizontal axis represents the location of the present coastline.

Here, however, we describe phase change using an error function between -1°C and 0°C . The shape of the freezing interval as we implemented it here holds an intermediate between the options more commonly used, as outlined in Kurylyk and Watanabe [2013], but smooths the end of the curve at 0°C which facilitates numerical solutions.

3. Boundary Conditions

The models described in this paper aim to be a generic and heuristic description of taliks under proglacial lakes surrounded by permafrost. However, the boundary conditions on taliks under lakes are loosely inspired by data from west Greenland near Kangerlussuaq (Figure 2), as the area is well studied [e.g., Scholz and Grottenthaler, 1988; Willemse, 2002; Dietrich *et al.*, 2005; Swedish Nuclear Fuel and Waste Management Company, 2011].

3.1. Glaciation History and Ice Sheet Geometry

The history of ice sheet buildup and collapse, and the topography of the ice sheet surface are the primary drivers of the hydraulic and thermal boundary conditions applied to the surface boundary representing hydrogeological forcing by the ice sheet. The history of ice sheet extent and thickness here are from inferred trends based upon field observations from west Greenland as reported by Greenland [Fleming and Lambeck, 2004]. The ice thickness (H [m]) is calculated using Paterson [1994]

$$H = AL^{0.5}, \quad (5)$$

in which A [-] is a scaling factor and L (m) is the distance from the ice margin. A ranges between 1 (for warm-based, soft-bedded ice) and 4.7 (for cold ice, resting on a solid bed) [Paterson, 1994]. For present-day

ice topography in west Greenland, A is estimated to be equal to ~ 3.5 which is the value we use in our modeling. In our model simulations, we assume that A is not variable in time.

After the LGM (at $\sim 15,000$ years B.P.), the west Greenland ice sheet margin retreated eastward by 175–200 km, interrupted by small readvances and reached the present-day position at around 6000 B.P. Between 6000 years B.P. and 4000 years B.P., the ice margin was east of the present-day position, with the ice sheet minimum occurring at around 4000 years B.P. around 60 km east of the present margin. This was followed by a readvance to the present-day position [van Tatenhoeve *et al.*, 1996; Scholz and Grottenthaler, 1988; Willemsen, 2002; Dietrich *et al.*, 2005]. We have included a simplified version of this glacial history in our model scenario buildup and retreat as follows. The ice sheet boundary in the model is set to retreat steadily from 15,000 years B.P. to 5000 years B.P., when the ice sheet retreated 50 km behind the present-day margin where it stays steady between 5000 years B.P. and 4000 years B.P. and readvances between 4000 years B.P. and 2000 years B.P. Thereafter, the ice location is kept constant and the model is run for an additional 4000 years [after Scholz and Grottenthaler, 1988, Figure 2]. The model is started at 16,000 years B.P. and spun up for 1000 years to 15,000 years B.P. and run for a total of 20,000 years to 4000 years in the future.

Uplift as a result of isostatic movement due to ice sheet retreat in the proglacial areas of the west Greenland ice sheet near Kangerlussuaq is roughly -3.1 mm a^{-1} ; while closer toward the coast, this rate is declining to a small subsidence of $\sim 1 \text{ mm a}^{-1}$ [Dietrich *et al.*, 2005]. The complexity of the ice sheet history in this area and the impact of this on present and past isostatic adjustments make it impossible to simply take the unloading rate of the last ice retreat to model current uplift rates as was, for example, assumed by Bense and Person [2008].

No sea level changes due to isostatic and eustatic processes are considered; as in the model the location of the sea is just representing a permafrost-free boundary. The investigation of the hydrogeological impacts of sea level changes goes beyond this study and is subject to further research.

In addition, no mechanical ice sheet loading is considered, because crystalline rocks used for the study described here have a very low compressibility and is thus neglected [Domenico and Schwarz, 1998; Vidstrand *et al.*, 2012].

3.2. Fluid Flow

Subglacial meltwater can recharge an aquifer when the glacier bed is wet-based. For west Greenland, subglacial temperatures at pressure melting have been suggested by models from Huybrechts [1996] and Brinkerhoff *et al.* [2011]. Subglacial water can either originate from in situ melt or during the melt season draining from the surface to the ice base, through crevasses, moulin, or englacial drainage structures [Zwally *et al.*, 2002]. Subglacial meltwater is generated by frictional heating between the glacier and the substratum or through ice movement and can result in a substantial amount of meltwater at the base of thermal parts of the glacier [Boulton *et al.*, 1993; Piotrowski, 2006]. Subglacial water leaves the glacier system through a combination of Darcian flow through the till, laminar flow through a water film at the ice bed interface, and through turbulent flow through conduits at the ice bed interface. Water discharges at the bed are generally too large to be discharged by groundwater flow only [Iverson and Person, 2012]. However, it has been suggested that if the ice sheet is underlain by a high permeability bedrock, such as carbonates, all meltwater can be drained through the bedrock. In contrast, if the glacier is underlain by a low permeability bedrock, efficient drainage through the bedrock is inhibited and high subglacial water pressures can build [Grasby and Chen, 2005]. This can then lead to channel flow and the formation of eskers [Boulton *et al.*, 1993]. Alternatively, meltwater exceeding the drainage capacity of the bedrock has been suggested to drain as a water film [Breemer *et al.*, 2002]. Hydraulic heads can be near flotation where the ice is underlain by a subglacial till with low permeability. The high water pressure and subglacial melting results in much larger groundwater recharge under thermal ice than that of present, ice-free conditions [Provost *et al.*, 2012]. For a crystalline glacier bed, fracture systems, often associated with fault zones, can provide the permeability required for substantial subglacial recharge.

To model the exchange of groundwater between the glacier bed and underlying aquifers, a flux boundary or a head boundary can be applied. A flux boundary condition based on estimated rates of basal melting may have an error of several orders of magnitudes, whereas setting the hydraulic head to the flotation value provides probably only a mild overestimate of actual heads at the bed surface [Iverson and Person, 2012]. Potentiometric head from paleo-pore water pressures are estimated as 72% of the ice thickness and have

been inferred from the stress characteristics of the fine-grained sediments [Piotrowski, 1997]. Lemieux *et al.* [2008a] argue that all meltwater reaching the glacier bed in excess of the flotation level of the ice sheet thickness should be treated as overland flow and leave the glacier through channelized flow, because, otherwise, the ice sheet would become unstable.

To account for the uncertainties in the hydraulic head value at the base of the ice sheet, two hydraulic head scenarios are considered here: a maximum hydraulic head value at ice flotation level and half the flotation level, following the ice sheet thickness by a factor of 0.9 and 0.45.

3.3. Heat Flow

The temperature distribution in the model is driven by the ground surface temperature at the top of the model domain, the basal heat flux at the base of the model, and heat advection due to groundwater movement (equation (4)). The mean annual air temperature for Kangerlussuaq during the period 1942–1992 was $-5.2 \pm 0.2^\circ\text{C}$ [van Tatenhove *et al.*, 1996]. However, ground surface temperatures differ from air temperatures due to the influence of slope, aspect, vegetation, soil type, duration, thickness, and properties of the snow cover. Borehole temperature profiles from DH-GAP03, approximately 1 km in front of the ice margin, suggest a mean annual ground surface temperature of -4.4°C before recent warming [Swedish Nuclear Fuel and Waste Management Company, 2011].

Lake water temperatures have been postulated to have been primarily driven by air temperature in the Kangerlussuaq area [D'Andrea *et al.*, 2011]. A sensitivity analysis of the ground surface temperature is carried out with ground surface temperatures set to -6 , -4 , and -2°C and a lake bottom temperature scenario to 0 , 2 , and 4°C to evaluate the thermal influence of driving surface temperatures on the existence of a talik under a lake.

The temperature at the base of the wet-based ice sheet is set to 0°C , thus ignoring any pressure effects on the melting temperature, which is in the order of 1.3°C under 2000 m of ice. The impact of supercooled water could be important to include in future research, as this might decrease the advective heat flow in the proglacial area. The temperature at the sea is set to 1°C to mimic a permafrost-free area.

In the model, surface temperatures are driven depending on the location of the ice margin with ground surface temperatures (GSTs) in the proglacial area and 0°C under the ice. Comparison of radiocarbon dates of shallow lake sediments and dating of moraines suggests lake development that coincides with the retreat of the ice sheet margin [Willemse, 2002]. Hence, lake formation in the Kangerlussuaq area is assumed to occur shortly after the local ice retreat. Thus, at the lake location the temperature is changed from surface temperature to lake bottom temperature (LBT) as soon as the ice has retreated locally.

The effects of variable density and viscosity in the calculated fluid flow field as a function of temperature and/or salinity are not taken into account. The effects of fluid properties on the regional flow field in this setting are not the primary focus of this study, and inclusion of these would require a different modeling approach. The chemical effects on freezing-point depression could have an influence on the permafrost distribution, as found in cryopegs, where supercooled brine water are found within the permafrost [Sloan and Van Everdingen, 1988].

3.4. Hydraulic and Thermal Properties of Bedrock

The possible impacts of the occurrence of till, lake sediments, and soil over bedrock have not been taken into account, and the properties of the model domain have been simplified to homogeneous bedrock. The thermal and hydraulic properties of bedrock are based on those for fractured crystalline rock (Table 1). Folded or sheared zones of Precambrian crystalline metamorphic rock have been estimated to have a hydraulic conductivity in the order of $10^{-8} (\text{m s}^{-1})$ [Swedish Nuclear Fuel and Waste Management Company, 2011]. A thermal conductivity of $2.7 (\text{W m}^{-1} \text{K}^{-1})$ is used to match the permafrost thickness of 335 m [Swedish Nuclear Fuel and Waste Management Company, 2011] for a steady state, conduction scenario. This value is in accordance with other measured thermal conductivities [Swedish Nuclear Fuel and Waste Management Company, 2011]. The volumetric heat capacity of bedrock is not given in this report, but a medium value for gneiss of $2.2 \cdot 10^6 (\text{J m}^{-3} \text{K}^{-1})$ is applied [Clauser, 2011].

3.5. Initial Conditions and Model Setup

The model domain is 2-D with depth of 1000 m and a width of 400 km, 100 km of fiord/sea and 300 km of ice, retreating 200 km since the LGM. To model heat flow, the sides of the model are nonflow and the base has a heat flux, q_{heat} . The sides and the base are no-flow boundaries for fluid flow (Figure 3).

Table 1. Hydraulic and Thermal Properties of Modeled Bedrock^a

Parameter	Symbol	Value	Units
Average matrix porosity	n	0.0048	—
Hydraulic conductivity in bedrock	K_0	10^{-8}	m s^{-1}
Specific storage of the aquifer	S_s	$10^{-6}/1.626 \cdot 10^{-4}$	m^{-1}
Volumetric heat capacity of water	C_w	$4220 \cdot 10^3$	$\text{J m}^{-3} \text{K}^{-1}$
Volumetric heat capacity of ice	C_i	$1835 \cdot 10^3$	$\text{J m}^{-3} \text{K}^{-1}$
Volumetric heat capacity of bedrock	C_s	$1875 \cdot 10^3$	$\text{J m}^{-3} \text{K}^{-1}$
Volumetric latent heat of fusion	L_i	$3.03 \cdot 10^8$	J m^{-3}
Heat flow density	q_{heat}	$34.8 \cdot 10^{-3}$	W m^{-2}
Gravitational acceleration	g	9.81	m s^{-2}

^aSymbols n , K_0 , and q_{heat} are measured in a borehole nearby (DH-GAP01) taken from Swedish Nuclear Fuel and Waste Management Company [2011].

The initial conditions are set during the LGM when the ice sheet terminated in the sea. The ground surface was insulated from the air temperatures, and there was no permafrost, as a wet-based ice sheet is assumed. When the ice retreats and the front terminates above the sea level, the ground surface gets exposed to subzero air temperatures and permafrost forms in the proglacial area.

Two sets of models are developed. Model A includes one lake and does not include isostatic rebound (Figure 3). This model is used to assess the relative importance of input parameters, and variations of model A are referred to as models A0 to A3. A conduction-only scenario is considered in models A0 and A1, where model A0 is a steady state model and A1 a transient model. Models A2 and A3 also consider heat advection, where the hydraulic head follows the ice sheet boundary by a factor of 0.45 and a factor of 0.9, respectively (Table 2). Models A2 and A3 are run for two scenarios for aquifer-specific storage: a lower value of 10^{-6} m^{-1} typical for crystalline bedrock [e.g., Domenico and Mifflin, 1965] (models A2-1 and A3-1) and a higher value of $1.6 \cdot 10^{-4} \text{ m}^{-1}$ measured near Kangerlussuaq [Swedish Nuclear Fuel and Waste Management Company, 2011] (models A2-2 and A3-2); however, this value is large for crystalline rock. Model A3-1-3 includes three lakes but is otherwise identical to model A3-1. Model B includes isostatic rebound after glacier retreat and includes Tóthian topography [Tóth, 1963]. The uplift rates are approximated from observed uplift, based on estimates [after Scholz and Grottenthaler, 1988, Figure 2a], and implemented as described in Figure 2b.

4. Results

This section presents model results showing talik evolution under a proglacial lake for a steady state, conduction model (A0), near a retreating ice sheet for a transient conduction model (A1), a transient conduction and advection model for different aquifer properties (A2 and A3) considering one lake and three lakes, and a transient conduction and advection model including isostatic uplift (B). Results are given in simulation time.

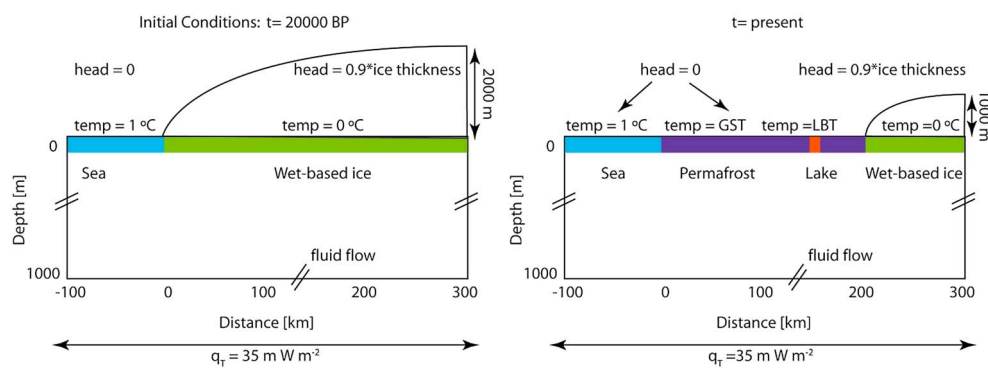


Figure 3. Initial and boundary conditions for hydraulic head and temperature. GST is ground surface temperature and LBT is lake bottom temperature.

Table 2. Description of Model Scenarios Used^a

Model	Type	S_s (m^{-1})
A0	steady state, heat conduction only	—
A1	transient, heat conduction only	—
A2-1	transient, coupled heat and fluid flow, head = $0.45 \cdot H$	10^{-6}
A2-2	transient, coupled heat and fluid flow, head = $0.45 \cdot H$	$1.626 \cdot 10^{-4}$
A3-1	transient, coupled heat and fluid flow, head = $0.9 \cdot H$	10^{-6}
A3-2	transient, coupled heat and fluid flow, head = $0.9 \cdot H$	$1.626 \cdot 10^{-4}$
A3-1-3	transient, coupled heat and fluid flow, head = $0.9 \cdot H$, 3 lakes	10^{-6}
B	transient, coupled heat and fluid flow, head = $0.9 \cdot H$, isostatic adjustment	10^{-6}

^a H denotes ice surface height.

4.1. Steady State, Heat Conduction-Only Model (A0)

In Figure 4, the permafrost distribution is presented for a lake with 100 m diameter for a steady state situation. Different temperature boundary conditions are used for the lake bottom temperature (LBT) ranging from 0°C to 4°C and with a ground surface temperature (GST) of -4°C. The boundary between permafrost and no-permafrost is defined as an ice saturation [-] of 0.95, whereas the ice saturation [-] ($\rho_i = \theta_i/n$) is defined as the ice content θ_i [-] divided by the porosity n [-]. When there is no thermal disturbance at the surface by the presence of a lake (black line), the permafrost thickness does not vary laterally. By introducing a 100 m wide lake with a LBT between 4°C and 0°C to the steady state model, the ground is insulated from air temperature and a talik forms under the lake.

Figure 5 presents the depth of the permafrost table and the permafrost base for different GST and LBT along a depth profile under the middle of the lake. In the absence of a lake (black line), permafrost depth for a steady state model ranges from 656 m to 130 m for GST of -10°C and -2°C, respectively. The presence, or absence, of permafrost underneath the lake is the crucial factor here, as this disables or enables a subpermafrost groundwater to surface water connection.

4.2. Transient, Heat Conduction Model (A1)

Modeled permafrost formation under a 100 m wide lake after ice retreat for one temperature scenario with a LBT of 1°C and a GST of -4°C is presented in Figure 6. Permafrost forms shortly after ice retreat at 8000 years of modeling time, which is when the ice retreats at the lake location. During the first years of the ground being exposed to subzero surface temperatures, permafrost forms at a larger rate than for subsequent years, which is evident from the permafrost thickness of ~85 m after the exposure

to GST for 250 years, and which is only doubled in 6000 years. The permafrost state under the lake center takes millennia to reach a steady state; 10,000 years since local ice retreat, permafrost is forming under the lake and 12,000 years since local ice retreat, and a steady state has not been reached yet with permafrost being approximately 30 m thinner than it should be for a steady state.

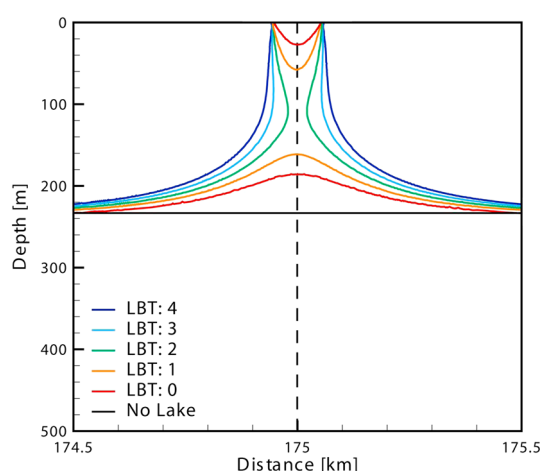


Figure 4. Permafrost distribution under a lake with different lake bottom temperatures (LBT) for a ground surface temperature (GST) of -4°C for a steady state, conduction-only model (A0).

4.3. Transient Conduction and Advection Model (A2 and A3)

Figure 7 presents model output of the ice sheet position, the discharge at the surface, the hydraulic head, and the temperature distribution for four different time steps for model A3. Groundwater is initially recharged under the ice sheet (Figure 7a, $t = 1000$ years). With ice retreat, groundwater discharges underneath the ice near the ice margin, as newly formed permafrost is inhibiting groundwater-surface

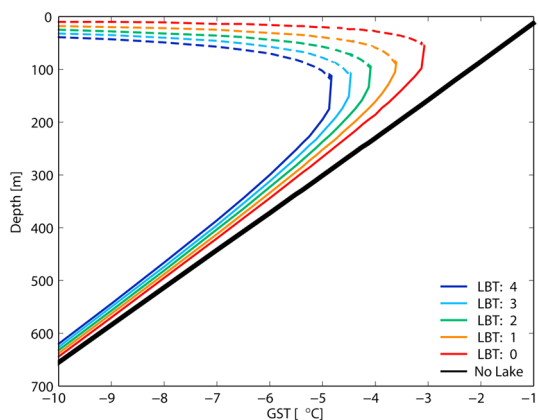


Figure 5. Depth of the permafrost base (solid line) and permafrost table (dashed line) under the center of a lake of 100 m diameter for a steady state, conduction-only permafrost model (A0). The black line represent the permafrost thickness with no thermal disturbance of a lake.

retreat and stagnation, implying that the system has not yet reached steady state (Figures 7 and A1k–A1n). When the ice sheet readvances, the regional hydraulic head gradient is forced by the position of the ice sheet, leading to an increase of discharge into the lake for models with relatively low aquifer-specific storage (A2-1 and A3-1), but this is not seen in models with a higher aquifer-specific storage (A2-2 and A3-2) (Figure A1). An open talik also results in a reversal of the groundwater flow direction near the lake, and groundwater flow closer to the sea is reversed and discharges into the talik (Figure 7b).

Once the talik has closed, the regional-scale groundwater flow direction is still reversed near the lake (Figure 7c). The zone where the groundwater flow lines converge shifts seaward until the location meets the groundwater divide, from which time all groundwater will flow toward the sea again (Figure 7d).

A more detailed distribution of the depth of the permafrost base, hydraulic head field, and flow vectors at the location of the lake is shown in Figure 8. When the lake is formed, the lake is subject to a low hydraulic head as defined by the land surface elevation, whereas a higher hydraulic head persists under the permafrost (Figure 8a). When the ground beneath the lake center is unfrozen, hydraulic head increases radially from the lake surface with exception of the surrounding permafrost, resulting in groundwater discharge into the lake. In the permafrost, the hydraulic heads are high, because the high hydraulic head values are preserved in the permafrost during permafrost formation from where they only very slowly dissipate.

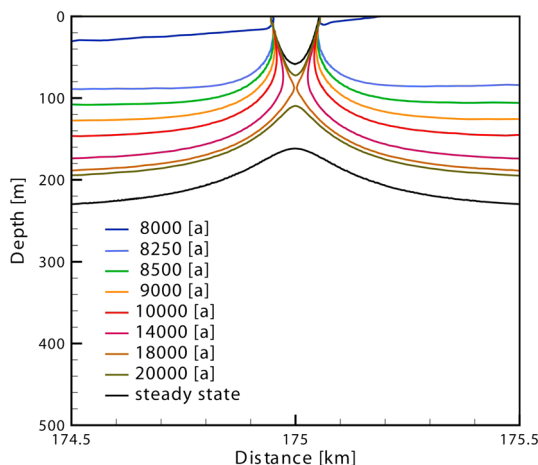


Figure 6. Permafrost formation over time under a lake with a lake bottom temperatures of 1°C and a ground surface temperature of –4°C for a transient, conduction-only model (A1).

water interaction in the proglacial area, except through taliks under lakes. For transient conduction and advection models (A2 and A3), permafrost formation follows the retreating ice and its thickness decreases gradually near the ice margin when the ice sheet is retreating (Figure 7b, $t = 10,000$ years). However, when the ice is advancing, the thickness of the permafrost increases steeply, as advective heat flow is largest near the ice margin and thermally erodes the permafrost (Figure 7c, $t = 15,000$ years).

Due to the very strong hydraulic head gradient near the ice margin, a vigorous local flow cell develops (Figure 7). However, this local groundwater flow system does not impact the discharge into the talik lake, which is driven by a regional-scale groundwater system. The magnitude of discharge into the lake decreases over time during ice sheet

This, however, does not influence groundwater flow, as the hydraulic conductivity in the permafrost is 8 orders of magnitude lower than in the unfrozen ground. Over time, the low hydraulic heads imposed at the lake location propagate radially into the subsurface resulting in a decrease of the hydraulic head gradient underneath the lake and thus a decrease in discharge into the lake. With decreasing discharge, the advective heat flow cooling the talik decreases, and when upward advective heat flow becomes less than the lateral conductive heat flow, the talik starts to freeze. Once the through talik has started to close, the groundwater convergence will shift in the direction of the talik. When the ground underneath the lake becomes partially frozen, the hydraulic head difference between the surface water and the subpermafrost aquifer in a depth profile under the lake increases by several tens of

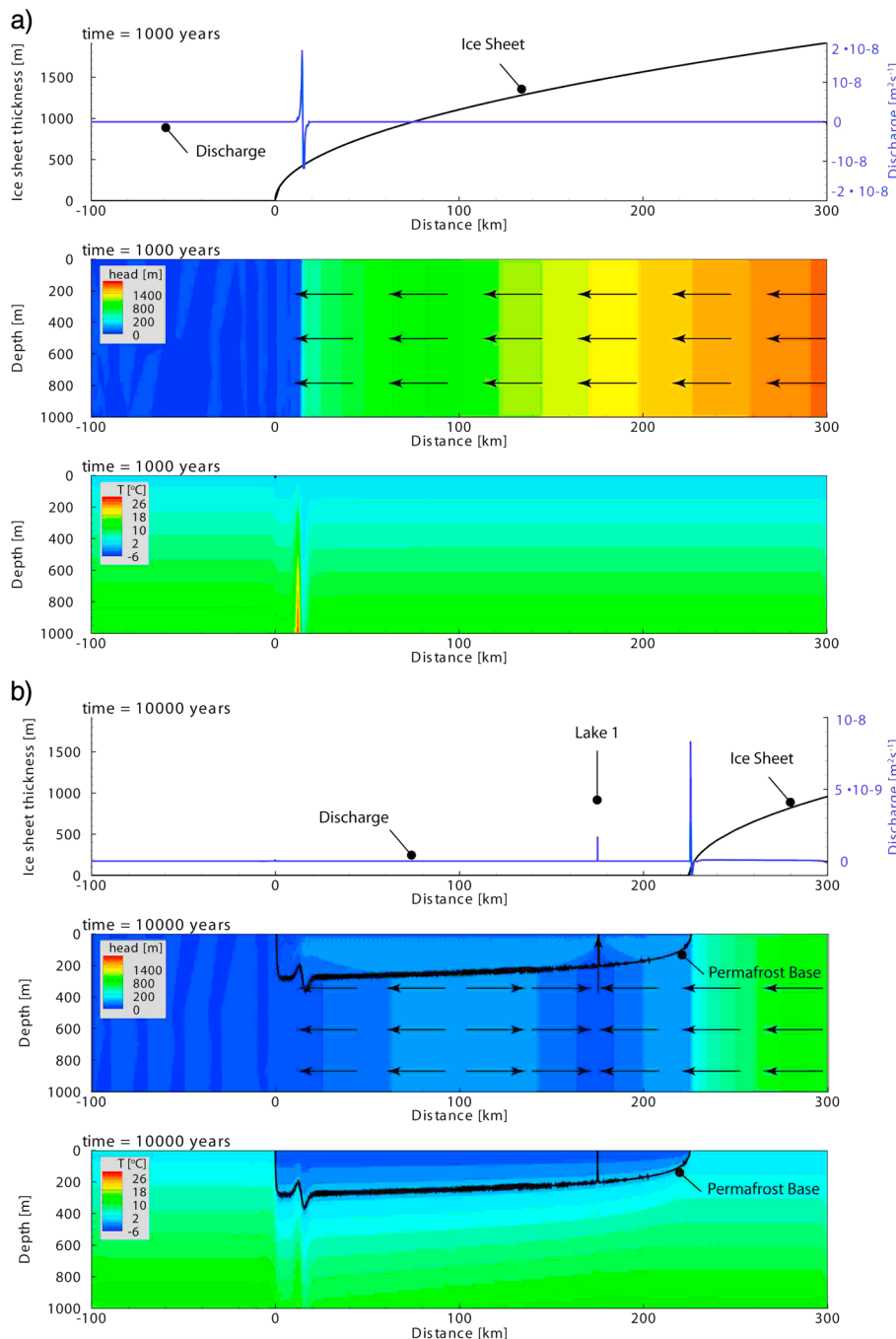


Figure 7. Modeled results for a transient conduction and advection scenario (model A3-1) with one lake of 100 m diameter. The first row presents the ice sheet location (black) and discharge to the surface (blue). The second row shows the hydraulic head field and flow vectors. The third row presents the temperature field and the permafrost base (black line). Result are presented for (a) 1000 years, (b) 10,000 years, (c) 12,500 years, and (d) 20,000 years simulation time. Models are run for a GST of -6°C and LBT of 4°C . The flow vectors are not to scale. The vertical exaggeration is 1:100.

meters (Figure 8b), controlled by larger-scale dynamics of the ice sheet position. However, as the hydraulic conductivity decreases with ice saturation, discharge into the lake decreases overall. Once the through talik has frozen through and the discharge into the lake has ceased, hydraulic heads underneath the permafrost increase (Figures 8c and 8d).

Figure 9 presents a depth profile under the lake center and 5 km away from the lake location, where the influence on hydraulic head and temperature of the lake should be negligible. Temperature (Figure 9a), ice

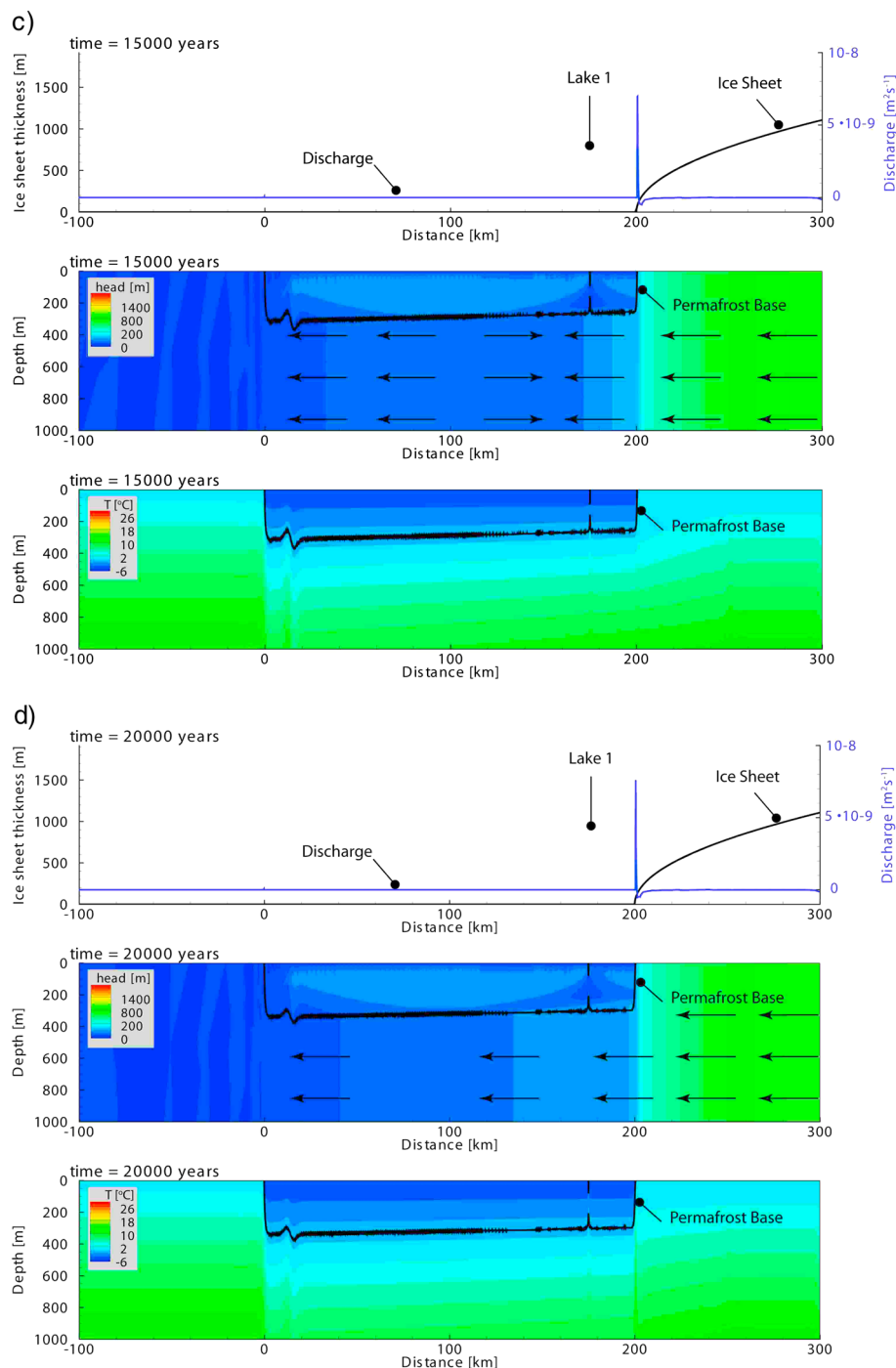


Figure 7. (continued)

saturation (Figure 9b), hydraulic head (Figure 9c), and vertical flow (Figure 9d) are presented for three different time steps of model A3-1 and the conduction-only steady state. Transient processes of heat storage of the bedrock, release and uptake of latent heat, and elastic release of groundwater with decreasing hydraulic heads result in heat flow large enough for a through talik to remain under the lake. In contrast, for a steady state situation considering only heat conduction, there is no through talik (Figures 9a and 9b). Hydraulic head is driven by the surface elevation and increases with depth, where the hydraulic head is influenced by the historic and current hydraulic head distribution near the ice margin. Hydraulic head differences in and under the permafrost are around twice as high as those under an open talik (Figure 9c); however, this does

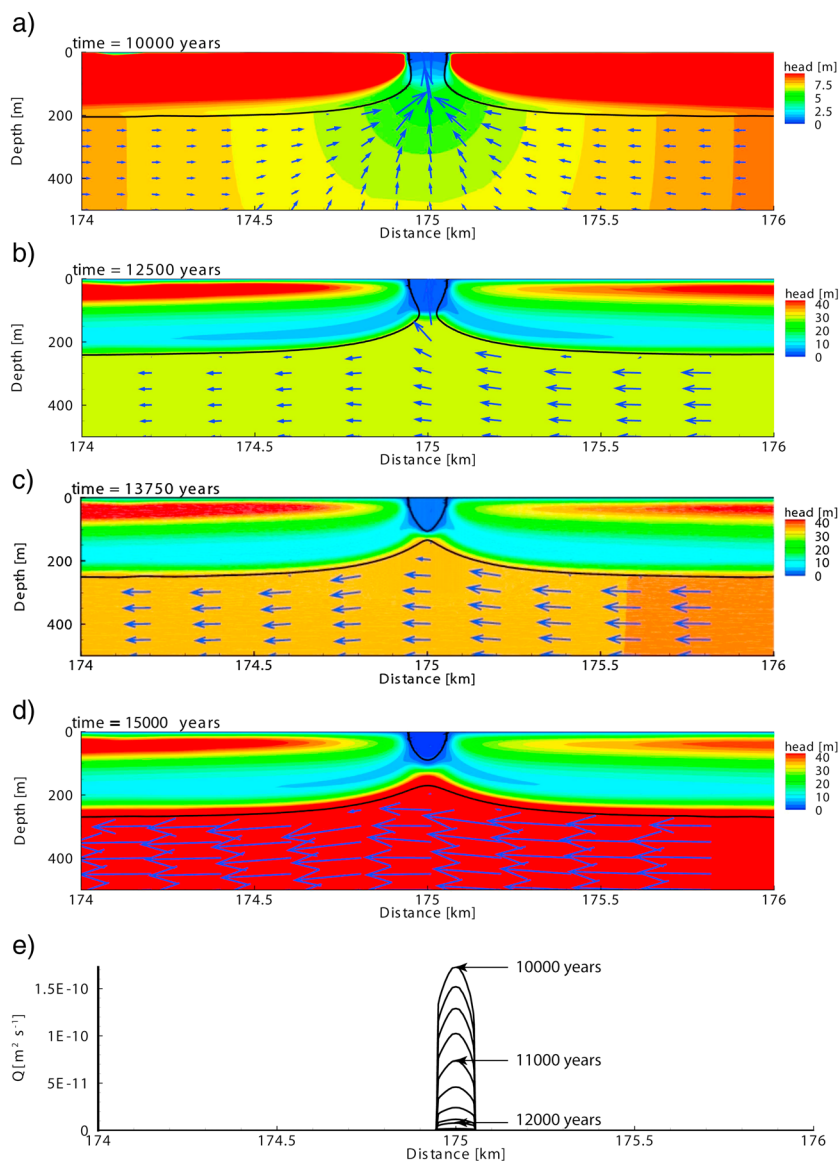


Figure 8. Detail of Figure 7 showing hydraulic head distribution, groundwater flow vectors, and permafrost base under a lake of 100 m diameter for a transient, conduction, and advection model (A3-1). Results are presented for (a) 10,000 years, (b) 12,500 years, (c) 13,750 years, (d) 15,000 years simulation time, and (e) discharge into the lake for a 250 year interval. Models are run for a GST of -6°C and LBT of 4°C . The flow vectors are not to scale.

not influence the groundwater flow, as hydraulic conductivities are several orders of magnitudes lower in the permafrost than in the unfrozen material. The hydraulic head difference in the open talik between the surface and at depth decreases over time which results in a decrease in vertical groundwater flow over time (Figure 9d).

The influence of advective heat transport on talik closure is demonstrated by comparing the conduction-only model (A1) with conduction and advection models (A2 and A3), for different aquifer properties, and is shown in Figure 10 for a GST of -6°C and LBT of 4°C (see Figure A1 for all model runs). For a lower specific aquifer storage of 10^{-6} m^{-1} , the influence of advective heat flow is relatively small. In this case the talik closure compared to the conduction-only scenario gets delayed by 350 years where the hydraulic head follows the ice sheet thickness by a factor of 0.45 (model A2-1) and 700 years for the scenario where the hydraulic head follows the ice sheet thickness by a factor of 0.9 (model A3-1). For a scenario of larger aquifer-specific storage of $1.6 \cdot 10^{-4} \text{ m}^{-1}$, the talik closure gets delayed compared to heat conduction by 4100 years for model A2-2 and does not freeze within the modeled time frame for model A3-2.

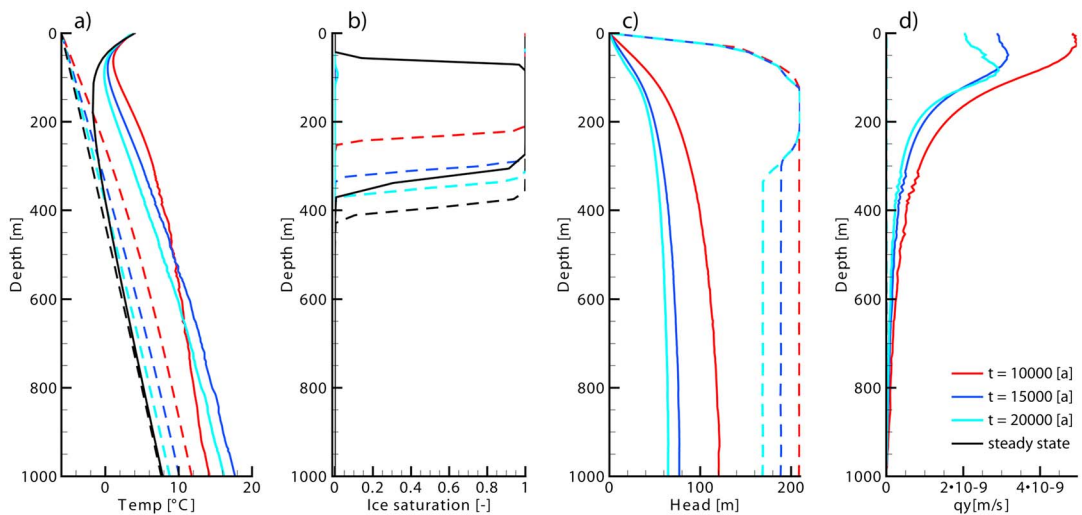


Figure 9. Profiles for (a) temperature, (b) ice saturation, (c) hydraulic head, and (d) vertical flow (q_y). The solid lines are for values under the middle of the talik and the dotted lines are for values 5 km next to the talik. Data shown are for a model run with GST of -6°C and a LBT of 4°C for model A3-1, and a steady state for model A0.

4.4. Effects of Several Open Taliks on the Regional Hydrogeology (Model A3-1-3)

In addition to the influence of the ice sheet history, the occurrence of more than one lake further influences the hydraulic head distribution, and as a consequence the larger-scale hydrogeology. As shown above, the existence of a through talik creates a hydraulic head minimum underneath an open talik, resulting in a reversal of the groundwater flow direction near the talik. Where there are several taliks adjacent to each other, the water divide occurs between two open taliks and convergences under each talik (Figure 11a). The high hydraulic head difference across the model domain under the permafrost decreases over time from up to tens of meters (Figure 11a) to meters (Figure 11b) and millimeters (Figure 11c).

4.5. Effects of Isostatic Uplift and Tóthian Topography on the Regional Hydrogeology (Model B)

The effect of isostatic uplift further complicates the hydraulic head distribution, as the hydraulic head follows the surface elevation (Figure 12). With uplift, the higher hydraulic heads, as defined on the surface, propagate through the unfrozen ground and respond to the current surface elevations. The propagation of the higher heads from the surface into the aquifer results in the lakes acting as a groundwater recharge into the aquifer and not as a groundwater discharge as in the models A2 and A3. Different uplift rates over

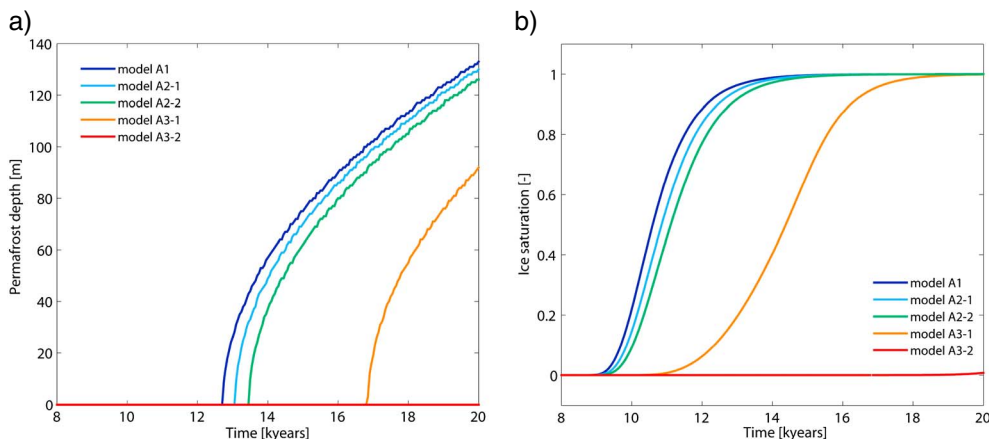


Figure 10. Comparison of (a) permafrost depth and (b) ice saturation of a talik of GST -6°C and LBT of 4°C for models with different hydraulic boundaries and aquifer properties as described in Table 2. Advective heat flow is larger for a higher aquifer-specific storage and higher hydraulic head gradients (model A3-2). Time is given in simulation time.

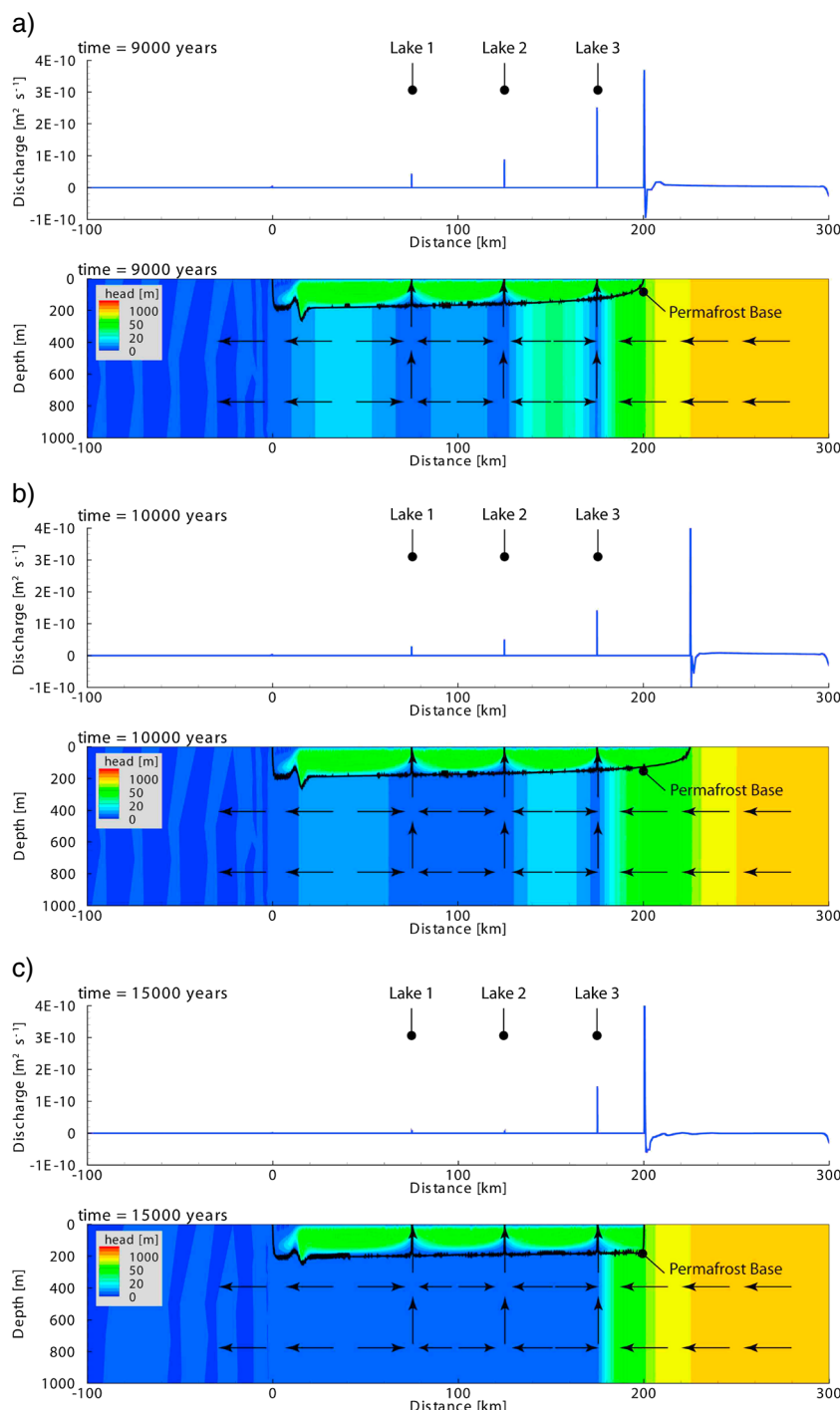


Figure 11. Surface discharge, hydraulic head, and permafrost distribution with three lakes at 75, 125, and 175 km of the model domain (model A3-1-3) for (a) 9000 years, (b) 10,000 years, and (c) 15,000 years of simulation time. Models are run for a GST of -4°C and LBT of 4°C . The flow vectors are not to scale.

the model domain result in spatially different rates of change of the hydraulic head distribution. In addition, relative higher hydraulic heads from nonpermafrost areas propagate underneath the permafrost, as can be observed at around distance = 80 km of the model domain (Figure 12).

The impact of the Tóthian topography [Tóth, 1963] as modeled here has a minor influence on the ground-water flow pattern.

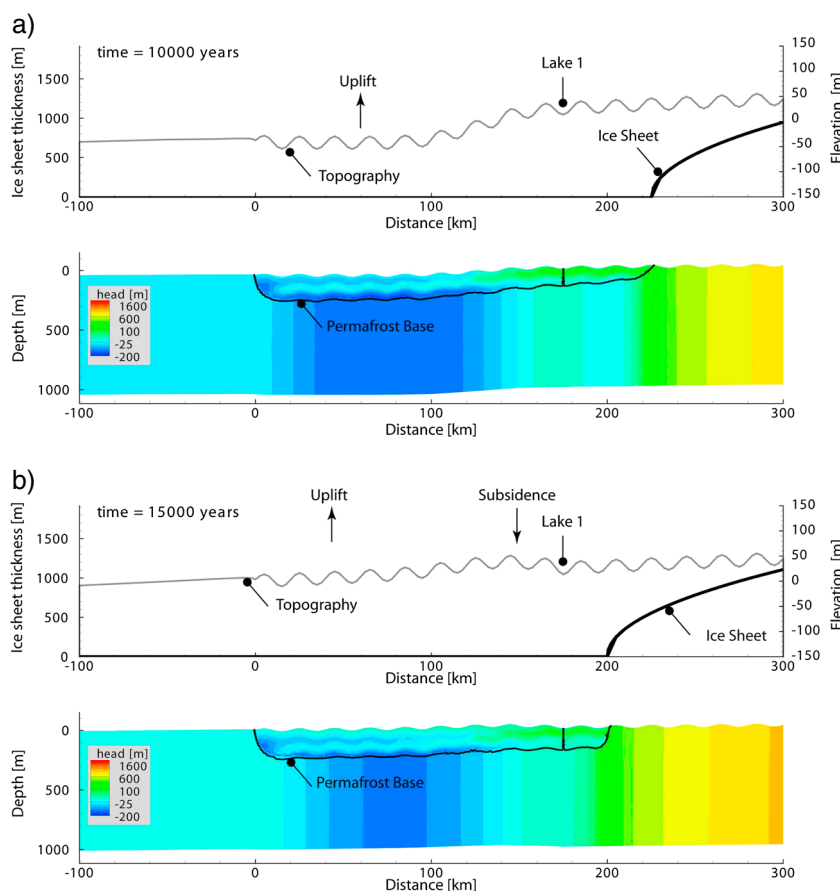


Figure 12. Permafrost depth, hydraulic head, and groundwater flow direction for a transient, conduction and advection including Tóthian topography and isostatic rebound (model B), for 10,000 years and 15,000 years simulation time. Models are run for a GST of -4°C and LBT of 4°C .

5. Discussion and Conclusion

This paper evaluates the influence of regional groundwater driven by ice sheet movement and associated advective heat transfer on the talik evolution of proglacial lakes since the LGM. This is done by comparison of simulated talik evolution under a proglacial lake for steady state and transient models including or excluding the effects of advective heat flow by groundwater flow.

The results from the models including advective heat flow demonstrate how local boundary conditions of a proglacial lake are controlled by larger-scale processes of a retreating ice sheet by determining the hydraulic and thermal boundary conditions at the surface. Groundwater discharge into the lake is mainly driven by an elastic storage response, releasing water from the bedrock aquifer after deglaciation (Figure 13). During a glaciation, hydraulic heads underneath the wet-based ice sheet are driven by the hydrostatic pressure of the ice sheet (Figure 13a). Higher hydraulic heads at depth than at the surface are preserved underneath the newly formed permafrost after deglaciation. When a talik forms, lower hydraulic head from the surface penetrates into the subsurface, resulting in a decreasing hydraulic head gradient (Figures 13b and 13c). In addition, high subglacial heads can propagate into the proglacial area. The hydraulic head gradient drives relatively warm subpermafrost groundwater to discharge through the talik into the lake. As long as the upward advective heat flow is larger than the lateral conductive heat flow cooling the talik from the sides, the permafrost is thermally eroded and the talik gets enlarged. Hence, when the upward advective heat flow decreases, the size of the talik decreases and eventually disappears (Figure 13c). We find that permafrost formation and change in hydraulic heads surrounding the talik interact, resulting in a complex pattern of hydraulic head gradients that changes over time. The models presented here considerably expand on the complexity of previous talik models under surface water bodies [Rowland *et al.*, 2011; Grenier *et al.*, 2013; Wellman *et al.*, 2013] which assume the hydraulic boundary conditions to be nonchanging over time.

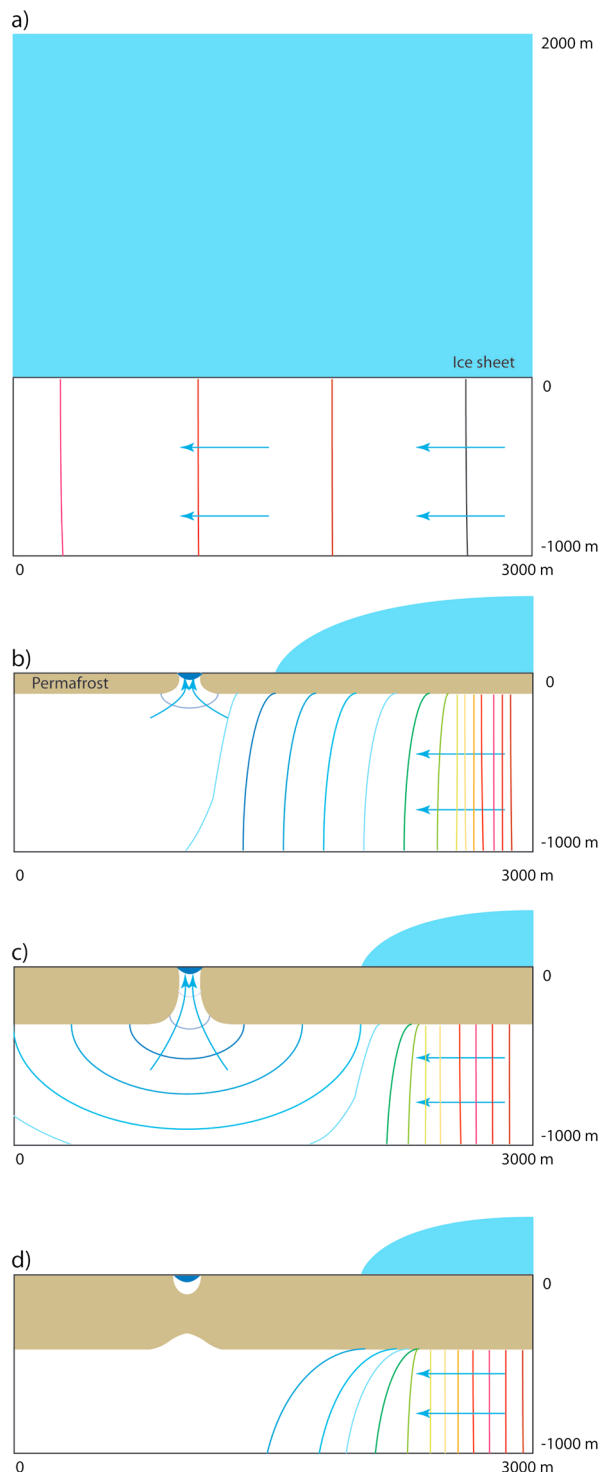


Figure 13. Conceptual model of the mechanism of groundwater discharge into a proglacial lake. The contours represent hydraulic head, whereas blue is low and red a high value. (a) During a glaciation, hydraulic heads underneath the wet-based ice sheet are high and are driven by the hydrostatic pressure of the ice sheet. (b and c) After ice retreat, the hydraulic heads at the surface have decreased by several 1000 m; however, the hydraulic head underneath the permafrost remain high. Through an open talik, low hydraulic heads penetrate and force groundwater to discharge into the lake. In addition, subglacial hydraulic heads propagate into the proglacial area. The duration of this groundwater discharge into the lake depends on the amount of elastic storage of groundwater from the previously ice-covered period. (d) Once groundwater flow has decreased to a critical threshold, advective heat flow is not large enough and the through talik will close. After the through talik has closed, the hydraulic heads increase again underneath the former through talik.

The talik geometry is primarily controlled by the thermal boundary conditions (model A1). These constitute the lake radius, the lake bottom temperature (LBT), the temperature of the surrounding permafrost, and the geothermal gradient govern the talik configuration. We did not vary lake size and geothermal gradient are not shown in this study, as we focus on ground surface temperature (GST) and LBT. However, for steady state models, an increase in LBT by 1°C can determine the presence or absence of ice of a depth profile under the lake center. This would imply that for small lakes for which the LBT follows GST, climate change and associated increase in LBT may decrease the permafrost thickness underneath the lake and may result in the formation of through taliks. However, comparing the transient conduction-only scenario (model A1) with the steady state conduction-only scenario (model A0) demonstrates that the permafrost formation under the lake has not yet reached a steady state for the transient models over a time scale of 12,000 years. Thus, this long response time to steady state conditions under lakes is an important factor to consider for larger-scale models. Examples include models that estimate permafrost distribution with a steady state (e.g., TTOP model) [Henry and Smith, 2001; Juliussen and Humlum, 2007] in regions with many lakes or steady state models that estimate ground temperatures under lakes [Mackay, 1962; Burn, 2002]. The latter type of models may seriously overestimate the permafrost thickness. Moreover, hydrogeological models that do not couple heat and fluid flow but prescribe the permafrost distribution [e.g. Bosson et al., 2012] may overestimate the permafrost distribution under surface water bodies.

In our model, the general groundwater flow direction is from the ice sheet toward the sea; however, taliks can locally reverse the groundwater flow direction creating a groundwater flow divide and a groundwater flow convergence at the talik. After talik closure, it will take several thousand years for the groundwater flow direction downstream of previous open taliks to reach its initial flow direction being from the ice sheet toward the sea (Figure 7). The larger-scale hydrogeology is thus affected by the existence of through taliks, and the occurrence of several open taliks can result in a complex hydrogeological pattern for several open through taliks (Figure 11).

The flow direction through taliks gets further complicated by the influence of isostatic uplift on the hydraulic head distribution (model B). Changes of the deeper hydraulic heads lag behind those at the surface. Therefore, uplift with associated higher hydraulic heads at the surface results in downwelling of groundwater through the talik (Figure 12). However, the influence of uplift and undulating topography as used in model B has a minor influence on the regional-scale hydrogeology. Although not considered here, it could be expected that the surface topography of deeper lakes and fjords would have a larger impact.

In addition to the thermal boundaries, advective heat flow can have a large impact on the closure time of a talik. This has been confirmed with lake talik models using a set hydraulic boundary [Rowland et al., 2011; Grenier et al., 2013], and groundwater flow has been hypothesized to have an equally dominant control on talik evolution as climatic drivers (e.g. surface temperature) [Wellman et al., 2013]. However, here we find that the magnitude of advective heat flow is strongly dependent on the amount of groundwater flow, which in a transient system as described here is dependent on the aquifer-specific storage and permeability. Depending on the aquifer properties, groundwater flow, and with it the associated advective heat flow component, has different response times to changing boundary conditions. An aquifer with a larger specific aquifer-specific storage responds slower to changing boundary conditions. Paleo effects of past ice sheet-driven hydrogeology can influence the hydrogeology for millennia [Bense and Person, 2008], whereas an aquifer with a smaller aquifer-specific storage is more sensitive to changing boundary conditions, and thus, the model reacts faster to the moving ice sheet and reaches a steady state more quickly. This can be observed by the effect of the advancing ice sheet on discharge into the lake, which is only visible for a lower aquifer-specific storage (10^{-6} m^{-1}), whereas for a higher aquifer-specific storage ($1.6 \cdot 10^{-4} \text{ m}^{-1}$) no clear change can be seen (Figure A1). This implies that for low-porosity rock with a low aquifer-specific storage the influence of advective heat flow is small and that the taliks are mainly "conductive taliks." However, for fissured and jointed rock as found in fault zones, advective heat flow is large and taliks are predominantly "advective-conductive taliks." Thus, a primary factor to consider for talik modeling is the aquifer-specific storage of an aquifer, which can range over several orders of magnitudes for crystalline rock [Domenico and Mifflin, 1965]. The importance of changing aquifer-specific storage with permafrost degradation and hydraulic head increase has been confirmed with numerical modeling, and uptake of groundwater into elastic aquifer storage has been found to be most profound for low permeability and high specific storage aquifers [Bense et al., 2012]. In the models presented here, an elastic release of groundwater with decreasing hydraulic heads after ice retreat is found.

Comparison of the model output with field observations is difficult for several reasons. First, field data enabling a direct comparison of permafrost occurrence are sparse and most temperature measurements are from boreholes [e.g., *Swedish Nuclear Fuel and Waste Management Company*, 2011]. An exception is the surveying with airborne electromagnetic imaging under lakes and rivers that provides a 3-D distribution of permafrost [Minsley et al., 2012; Jepsen et al., 2013]. Geochemical analysis [e.g., Clark et al., 2001; Stotler et al., 2011; Utting et al., 2012] can provide evidence for groundwater sources in surface water bodies. However, modeling input parameters, such as hydraulic head distribution, hydraulic conductivities, and their spacial distribution are usually unknown.

Further to the uncertainties in model input parameters, uncertainties in processes covered and transfer functions describing ice saturation or permeability reduction over the freezing interval complicate a direct comparison [Ireson et al., 2013]. The timing of permafrost thaw or formation is also influenced by the definition of the temperature interval over which freeze/thaw occurs, with a wider freezing interval leading to later, and a narrower freezing interval leading to earlier talik closure [McKenzie et al., 2007]. In addition, the impacts of mechanical loading and unloading by the ice sheet are not included in this study, which impacts the fluid pressures in previously ice covered areas [Bense and Person, 2008]. However, the compressibility values for crystalline rocks applied in this study are very low [Domenico and Schwarz, 1998; Vidstrand et al., 2012] and were therefore neglected.

This model can be applied to regions of crystalline bedrock in front of a dynamic ice sheet that has been wet-based for the whole simulation period, which is valid for most of Greenland [Huybrechts, 1996]. Where the glacier is polythermal (e.g., Arctic Canada and Svalbard), recharge only occurs in the wet-based parts of the glaciers and where there is no permafrost underlying the ice. For those regions, a model like the one used here will thus probably overestimate rates of subglacial recharge. The models described here are valid for a lake that formed immediately after ice retreat, which has been observed in west Greenland [Willemse, 2002].

Ongoing climate change can influence talik systems in several ways. First, ground surface temperature increase and increase of the lake bottom temperature will lead to the formation of more hydraulically conductive through taliks, enabling a groundwater surface water connection. These new through taliks may then shift the general groundwater flow direction near the talik to discharge into the lake. Second, with ice sheet dynamics, hydraulic head gradients will alter and will thus affect the groundwater recharge and the hydraulic head distribution at near ice-marginal positions. Third, glacier thinning may result in the glacier bed thermal regime becoming cold-based, inhibiting any further recharge. This has been observed at Ester mine spring in Svalbard, where the spring discharge ceased after the recharging glacier had become cold-based [Haldorsen et al., 2010]. Fourth, new regions will become ice free, enhancing the potential for more proglacial lakes to develop.

This study shows that permafrost regions in front of glaciers and ice sheets might be hydrogeologically active and that strong vertical fluxes through taliks under surface water bodies can occur. This enables the transport of pollutants from mining; as for example, mines for rare Earth minerals and zinc are becoming increasingly popular in Greenland, and uranium-thorium mining is being considered [Geological Survey of Denmark and Greenland and Bureau of Minerals and Petroleum, 2011, 2013]. In addition, these types of models can be used for assessing the potential of groundwater movement around potential nuclear waste storage sites under future glaciation scenarios.

In summary, in this study we find that in glaciated regions near an ice margin the hydrogeology is complex and transient and cannot be modeled with a static hydraulic head boundary. In addition, advective heat flow can be large depending on the aquifer properties and through taliks can exist in areas where heat conduction only would not suggest a through talik.

Appendix A: Complete Sensitivity Study of Modeling Scenarios

Figure A1 presents the complete sensitivity study for permafrost depth, ice saturation and discharge for a conduction-only scenario (model A1), and for conduction and advection scenarios for different hydraulic boundaries and aquifer properties as described in Table 2. Ground surface temperatures (GSTs) of -6°C , -4°C , and -2°C and lake bottom temperatures (LBTs) of 4°C , 2°C , and 0°C are used.

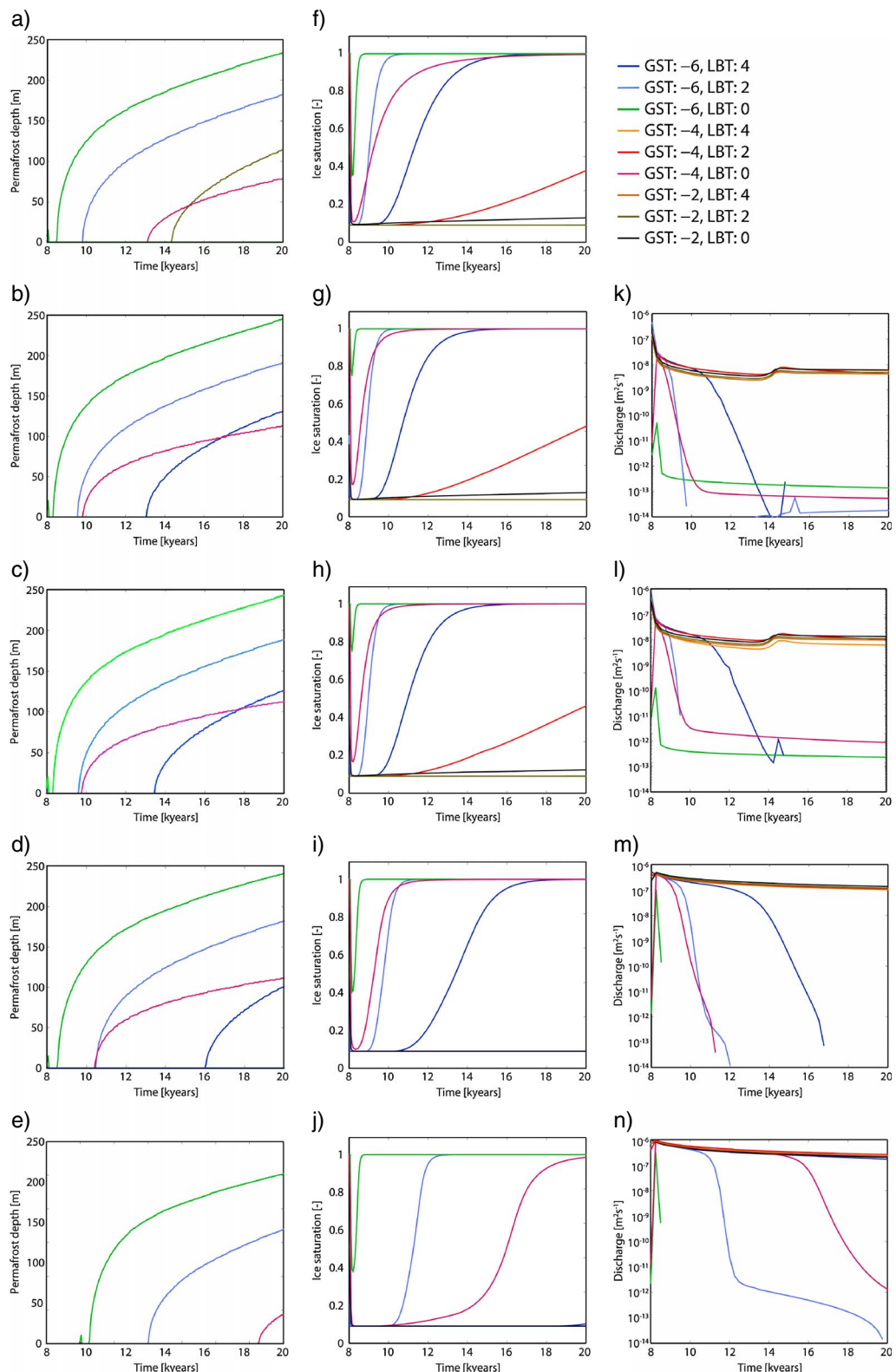


Figure A1. (a–e) Permafrost depth under a lake of 100 m diameter. (f–j) Maximum ice saturation under a lake of 100 m diameter. (k–n) Discharge into the lake. Permafrost is defined as 0.95 ice saturation. GST is ground surface temperature, and LBT is lake bottom temperature. All models are for a transient conduction only (model A1) and transient conduction and advection model (model A2 and A3) for a lower specific aquifer ($S_s = 10^{-6} [\text{m}^{-1}]$) storage and a higher specific aquifer storage ($S_s = 1.6 \cdot 10^{-4} [\text{m}^{-1}]$). Time is given in simulation time.

Modeling permafrost formation under a 100 m wide lake after ice retreat for different lake bottom temperatures and ground surface temperatures considering heat conduction only shows that for a GST of $< -6^{\circ}\text{C}$ all taliks freeze through between a few hundred years (LBT of 0°C) and up to 6000 years (LBT of 4°C) after ice retreat. For a GST of -4°C , only the talik with a LBT of 0°C freezes through (Figure A1a). The freezing process of the taliks occurs over different time spans, depending on the LBTs; for a low LBT, the talik freezes through quickly (hundred years), and for a higher LBT, the freezing process occurs over several thousand years. For two cases, lakes with a GST of -4°C and LBT of 2°C , as well as -2°C and 0°C , respectively, are partially frozen and have not reached steady state during the modeling time (Figure A1f).

Permafrost depth, ice saturation, and discharge under a lake of 100 m diameter over time for GST ranging from -2°C to -6°C , LBT from 0°C to 4°C , and for a hydraulic head boundary following the ice thickness by a factor of 0.45 (model A2) and 0.9 (model A3) are presented in Figures A1b–A1e and A1g–A1n. Discharge generally decreases over time but peaks when the ice sheet readvances, responding to the regional hydraulic head gradients forced by the position of the ice sheet. The magnitude of discharge first decreases, then the maximum ice saturation increases. When the ice saturation increases, discharge is decreasing at a faster rate and ceases. The permafrost formation under these lakes differs for model A2 and model A3; a higher head delays the freezing process. Using larger aquifer-specific storage has the largest influence on the timing of permafrost formation.

Acknowledgments

Sylvi Holdorsen and three anonymous reviewers are thanked for their constructive comments to improve the quality of this manuscript.

References

- Andersen, D. T., W. H. Pollard, C. P. McKay, and J. Heldmann (2002), Cold springs in permafrost on Earth and Mars, *J. Geophys. Res.*, 107(E3), 5015, doi:10.1029/2000JE001436.
- Bense, V. F., and M. A. Person (2008), Transient hydrodynamics within intercratonic sedimentary basins during glacial cycles, *J. Geophys. Res.*, 113, F04005, doi:10.1029/2007JF000969.
- Bense, V. F., G. Ferguson, and H. Kooi (2009), Evolution of shallow groundwater flow systems in areas of degrading permafrost, *Geophys. Res. Lett.*, 36, L22401, doi:10.1029/2009GL039225.
- Bense, V. F., H. Kooi, G. Ferguson, and T. Read (2012), Permafrost degradation as a control on hydrogeological regime shifts in a warming climate, *J. Geophys. Res.*, 117, F03036, doi:10.1029/2011JF002143.
- Bosson, E., U. Sabel, L.-G. Gustafsson, M. Sassner, and G. Destouni (2012), Influences of shifts in climate, landscape, and permafrost on terrestrial hydrology, *J. Geophys. Res.*, 117, D05120, doi:10.1029/2011JD016429.
- Boulton, G. S., T. Slot, K. Blessing, P. Glasbergen, T. Leijnse, and K. van Gijssel (1993), Deep circulation of groundwater in overpressured subglacial aquifers and its geological consequences, *Quat. Sci. Rev.*, 12(9), 739–745, doi:10.1016/0277-3791(93)90014-D.
- Breemer, C., P. Clark, and R. Haggerty (2002), Modeling the subglacial hydrology of the late Pleistocene Lake Michigan Lobe, Laurentide Ice Sheet, *Geol. Soc. Am. Bull.*, 114(6), 665–674, doi:10.1130/0016-7606(2002)114<0665:MTSHOT>2.0.CO;2.
- Brinkerhoff, D. J., T. W. Meierbacholt, J. V. Johnson, and J. T. Harper (2011), Sensitivity of the frozen/melted basal boundary to perturbations of basal traction and geothermal heat flux: Isunnguita Sermia, western Greenland, *Ann. Glaciol.*, 52(59), 43–50, doi:10.3189/172756411799096330.
- Burn, C. R. (2002), Tundra lakes and permafrost, Richards Island, western Arctic coast, Canada, *Can. J. Earth Sci.*, 39(8), 1281–1298, doi:10.1139/E02-035.
- Cardenas, M. B., and X.-W. Jiang (2010), Groundwater flow, transport, and residence times through topography-driven basins with exponentially decreasing permeability and porosity, *Water Resour. Res.*, 46, W11538, doi:10.1029/2010WR009370.
- Clark, I., B. Lauriol, L. Harwood, and M. Marschner (2001), Groundwater contributions to discharge in a permafrost setting, Big Fish River, N.W.T., Canada, *Arct. Antarct. Alp. Res.*, 33, 62–69, doi:10.2307/1552278.
- Clauser, C. (2011), Thermal storage and transport properties of rocks, I: Heat capacity and latent heat, in *Encyclopedia of Solid Earth Geophysics*, edited by H. Gupta, pp. 1423–1431, Springer, Dordrecht.
- Cutler, P. M., D. R. MacAyeal, D. M. Mickelson, B. R. Parizek, and P. M. Colgan (2000), A numerical investigation of ice-lobe-permafrost interaction around the southern Laurentide ice sheet, *J. Glaciol.*, 46(153), 311–325, doi:10.3189/172756500781832800.
- D'Andrea, W. J., Y. Huang, S. C. Fritz, and N. J. Anderson (2011), Abrupt holocene climate change as an important factor for human migration in West Greenland, *Proc. Natl. Acad. Sci. U.S.A.*, 108, 9765–9769, doi:10.1073/pnas.1101708108.
- Dietrich, R., A. Rulke, and M. Scheinert (2005), Present-day vertical crustal deformations in West Greenland from repeated GPS observations, *Geophys. J. Int.*, 163(3), 865–874, doi:10.1111/j.1365-246X.2005.02766.x.
- Domenico, P., and F. Schwarz (1998), *Physical and Chemical Hydrogeology*, John Wiley, N.Y.
- Domenico, P. A., and M. Mifflin (1965), Water from low-permeability sediments and land subsidence, *Water Resour. Res.*, 1(4), 563–576.
- Fleming, K., and K. Lambeck (2004), Constraints on the Greenland Ice Sheet since the Last Glacial Maximum from sea-level observations and glacial-rebound models, *Quat. Sci. Rev.*, 23(9–10), 1053–1077, doi:10.1016/j.quascirev.2003.11.001.
- Ge, S., J. McKenzie, C. Voss, and Q. Wu (2011), Exchange of groundwater and surface-water mediated by permafrost response to seasonal and long term air temperature variation, *Geophys. Res. Lett.*, 38, L14402, doi:10.1029/2011GL047911.
- Geological Survey of Denmark and Greenland, and Bureau of Minerals and Petroleum (2011), MINEX: Greenland Mineral Exploration Newsletter, *MINEX*, 40, 1–8.
- GEUS, and BMP (2013), MINEX: Greenland Mineral Exploration Newsletter, *MINEX*, 43, 1–8.
- Grasby, S., and Z. Chen (2005), Subglacial recharge into the Western Canada Sedimentary Basin - Impact of Pleistocene glaciation on basin hydrodynamics, *Geol. Soc. Am. Bull.*, 117(3–4), 500–514, doi:10.1130/B25571.1.
- Grasby, S. E., B. Beauchamp, and V. Bense (2012), Sulfuric acid Speleogenesis associated with a glacially driven groundwater system-paleo-spring "pipes" at Borup Fiord Pass, Nunavut, *Astrobiology*, 12(1), 19–28, doi:10.1089/ast.2011.0700.
- Grenier, C., D. Régner, E. Mouche, H. Benabderrahmane, F. Costard, and P. Davy (2013), Impact of permafrost development on groundwater flow patterns: A numerical study considering freezing cycles on a two-dimensional vertical cut through a generic river-plain system, *Hydrogeol. J.*, 21(1), 257–270, doi:10.1007/s10040-012-0909-4.

- Haldorsen, S., M. Heim, B. Dale, J. Y. Landvik, M. van der Ploeg, A. Leijnse, O. Salvigsen, J. Hagen, and D. Banks (2010), Sensitivity to long-term climate change of subpermafrost groundwater systems in Svalbard, *Quat. Res.*, 73(2), 393–402, doi:10.1016/j.yqres.2009.11.002.
- Henry, K., and M. Smith (2001), A model-based map of ground temperatures for the permafrost regions of Canada, *Permafrost Periglac. Process.*, 12(4), 389–398, doi:10.1002/ppp.399.
- Huybrechts, P. (1996), Basal temperature conditions of the Greenland ice sheet during the glacial cycles, *Ann. Glaciol.*, 23, 226–236.
- Ireson, A. M., G. van der Kamp, G. Ferguson, U. Nachshon, and H. S. Wheater (2013), Hydrogeological processes in seasonally frozen northern latitudes: Understanding, gaps and challenges, *Hydrogeol. J.*, 21, 53–66, doi:10.1007/s10040-012-0916-5.
- Iverson, N., and M. Person (2012), Glacier-bed geomorphic processes and hydrologic conditions relevant to nuclear waste disposal, *Geofluids*, 12(1), 38–57, doi:10.1111/j.1468-8123.2011.00355.x.
- Jepsen, S. M., C. I. Voss, M. A. Walvoord, B. J. Minsley, and J. Rover (2013), Linkages between lake shrinkage/expansion and sub-lacustrine permafrost distribution determined from remote sensing of interior Alaska, USA, *Geophys. Res. Lett.*, 40, 882–887, doi:10.1002/grl.50187.
- Jiang, X.-W., L. Wan, X.-S. Wang, S. Ge, and J. Liu (2009), Effect of exponential decay in hydraulic conductivity with depth on regional groundwater flow, *Geophys. Res. Lett.*, 36, L24402, doi:10.1029/2009GL041251.
- Juliussen, H., and O. Humlum (2007), Towards a TTOP ground temperature model for mountainous terrain in central-eastern Norway, *Permafrost Periglac. Process.*, 18(4), 161–184, doi:10.1002/ppp.586.
- Kleinberg, R. L., and D. D. Griffin (2005), NMR measurements of permafrost: Unfrozen water assay, pore-scale distribution of ice, and hydraulic permeability of sediments, *Cold Reg. Sci. Technol.*, 42(1), 63–77, doi:10.1016/j.coldregions.2004.12.002.
- Kukkonen, I., L. Kivekäs, S. Vuorilainen, and M. Kääriä (2011), Thermal properties of rocks in Olkiluoto: Results of laboratory measurements 1994–2010, *WR 2011–17*, Geological Survey of Finland.
- Kurylyk, B., and K. Watanabe (2013), Review: The mathematical representation of freezing and thawing processes in variably saturated, non-deformable soils, *Adv. Water Resour.*, 60, 160–177, doi:10.1016/j.advwatres.2013.07.016.
- Lemieux, J.-M., E. A. Sudicky, W. R. Peltier, and L. Tarasov (2008a), Dynamics of groundwater recharge and seepage over the Canadian landscape during the Wisconsinian glaciation, *J. Geophys. Res.*, 113, F01011, doi:10.1029/2007JF000838.
- Lemieux, J.-M., E. A. Sudicky, W. R. Peltier, and L. Tarasov (2008b), Simulating the impact of glaciations on continental groundwater flow systems: 1. Relevant processes and model formulation, *J. Geophys. Res.*, 113, F03017, doi:10.1029/2007JF000928.
- Lemieux, J.-M., E. A. Sudicky, W. R. Peltier, and L. Tarasov (2008c), Simulating the impact of glaciations on continental groundwater flow systems: 2. Model application to the Wisconsinian glaciation over the Canadian landscape, *J. Geophys. Res.*, 113, F03018, doi:10.1029/2007JF000929.
- Ling, F., and T. Zhang (2003), Numerical simulation of permafrost thermal regime and talik development under shallow thaw lakes on the Alaskan Arctic Coastal Plain, *J. Geophys. Res.*, 108(D16), 4511, doi:10.1029/2002JD003014.
- Mackay, J. R. (1962), Pingos of the Pleistocene Mackenzie delta area, *Geogr. Bull.*, 18, 21–63.
- McKenzie, J. M., C. I. Voss, and D. I. Siegel (2007), Groundwater flow with energy transport and water-ice phase change: Numerical simulations, benchmarks, and application to freezing in peat bogs, *Adv. Water Resour.*, 30(4), 966–983, doi:10.1016/j.advwatres.2006.08.008.
- Minsley, B., et al. (2012), Airborne electromagnetic imaging of discontinuous permafrost, *Geophys. Res. Lett.*, 39, L02503, doi:10.1029/2011GL050079.
- Paterson, W. S. B. (1994), *The Physics of Glaciers*, 3rd ed., Butterworth-Heinemann, Oxford.
- PDE Solutions (2006), FlexPDE v.5.10, PDE Solutions, Spokane Valley, Wash. [Available at <http://www.pdesolutions.com>.]
- Piotrowski, J. A. (1997), Subglacial hydrology in north-western Germany during the last glaciation: Groundwater flow, tunnel valleys and hydrological cycles, *Quat. Sci. Rev.*, 16(2), 169–185, doi:10.1016/S0277-3791(96)00046-7.
- Piotrowski, J. A. (2006), Groundwater under ice sheets and glaciers, in *Glacier Science and Environmental Change*, edited by P. G. Knight, pp. 50–59, Blackwell, Malden, Mass.
- Provost, A. M., C. I. Voss, and C. E. Neuzil (2012), Glaciation and regional groundwater flow in the Fennoscandian shield, *Geofluids*, 12, 79–96, doi:10.1111/j.1468-8123.2012.00361.x.
- Rowland, J. C., B. J. Travis, and C. J. Wilson (2011), The role of advective heat transport in talik development beneath lakes and ponds in discontinuous permafrost, *Geophys. Res. Lett.*, 38, L17504, doi:10.1029/2011GL048497.
- Scheidegger, J. M., V. F. Bense, and S. E. Grasby (2012), Transient nature of Arctic spring systems driven by subglacial meltwater, *Geophys. Res. Lett.*, 39, L12405, doi:10.1029/2012GL051445.
- Scholz, H., and W. Grottenthaler (1988), Beiträge zur jungholozänen Deglaziationsgeschichte im mittleren Westgrönland, *Polarforschung*, 58(1), 25–40.
- Swedish Nuclear Fuel and Waste Management Company (2011), The Greenland Analogue Project Yearly Report 2010, *Tech. Rep. SKB R-11-23*, Swedish Nuclear Fuel and Waste Manage Co.
- Sloan, C., and R. Van Everdingen (1988), Region 28, Permafrost region, in *Hydrogeology, Geology of North America*, pp. 263–270, Geol. Soc. of Am., Boulder, Colo.
- Stottler, R., S. Frape, B. Freifeld, B. Holden, T. Onstott, T. Ruskeeniemi, and E. Chan (2011), Hydrogeology, chemical and microbial activity measurement through deep permafrost, *Ground Water*, 49(3), 348–364, doi:10.1111/j.1745-6584.2010.00724.x.
- Tóth, L. (1963), A theoretical analysis of groundwater flow in small drainage basins, *J. Geophys. Res.*, 68(16), 4795–4812.
- Utting, N., I. Clark, B. Lauriol, M. Wieser, and W. Aeschbach-Hertig (2012), Origin and flow dynamics of perennial groundwater in continuous permafrost terrain using isotopes and noble gases: Case study of the Fishing Branch River, Northern Yukon, Canada, *Permafrost Periglac. Process.*, 23(2), 91–106, doi:10.1002/ppp.1732.
- van Tatenhove, F., A. Fabre, R. Greve, and P. Huybrechts (1996), Modelled ice-sheet margins of three Greenland ice-sheet models compared with a geological record from ice-marginal deposits in central West Greenland, *Ann. Glaciol.*, 23, 52–58.
- Vidstrand, P., S. Follin, J.-O. Selroos, J.-O. Näslund, and I. Rhén (2012), Modeling of groundwater flow at depth in crystalline rock beneath a moving ice-sheet margin, exemplified by the Fennoscandian Shield, Sweden, *Hydrogeol. J.*, 21, 239–255, doi:10.1007/s10040-012-0921-8.
- Wellman, T. P., C. I. Voss, and M. Walvoord (2013), Impacts of climate, lake size, and supra- and sub-permafrost groundwater flow on lake-talik evolution, Yukon Flats, Alaska (USA), *Hydrogeol. J.*, 21, 281–298, doi:10.1007/s10040-012-0941-4.
- Willemse, N. (2002), *Holocene Sedimentation History of the Shallow Kangerlussuaq Lakes, West Greenland*, Meddelelser om Grönland, Geoscience, vol. 41, Danish Polar Center, Copenhagen.
- Zwally, H. J., W. Abdalati, T. Herring, K. Larson, J. Saba, and K. Steffen (2002), Surface melt-induced acceleration of Greenland ice-sheet flow, *Science*, 297, 218–222, doi:10.1126/science.1072708.